3D grid codes in human entorhinal cortex: Theoretical and methodological considerations and fMRI findings

Misun Kim, Eleanor A. Maguire

Wellcome Centre for Human Neuroimaging, Institute of Neurology, University College London, London WC1N 3AR, UK

Corresponding author: Eleanor A. Maguire
Wellcome Centre for Human Neuroimaging, Institute of Neurology, University College London, 12 Queen Square, London WC1N 3AR, UK; e.maguire@ucl.ac.uk
Tel: +44 020 3448 4362
Fax: +44 020 7813 1445

Abstract

Recent human functional magnetic resonance imaging (fMRI) and animal electrophysiology studies suggest that grid cells in entorhinal cortex are an efficient neural mechanism for encoding knowledge about the world, not only for spatial location but also for more abstract cognitive information. The world, be it physical or abstract, is often high-dimensional. However, grid cells have been mainly studied on a simple two-dimensional (2D) plane and little is known about how grid cells encode the three-dimensional (3D) physical space in which we live. This dearth of knowledge is partly due to the technical difficulty of recording freely moving animals in 3D. Here, we first developed interactive software to help researchers visualize 3D grid fields and predict the grid activity in 3D. This relies on the known property of grid cells where their activity is modulated by the movement direction of animals relative to the grid axis. We then searched for 3D grid-like signals in human entorhinal cortex using a novel 3D virtual reality paradigm and a new fMRI analysis method. We found that signals in the left entorhinal cortex were explained by a face-centred cubic lattice model. This is the first empirical evidence for 3D grid codes in the human brain, notwithstanding the inherent methodological limitations of fMRI. We believe that our findings and software serve as a useful initial stepping-stone for studying grid cells in realistic 3D worlds and also, potentially, for interrogating abstract high-dimensional cognitive processes.

Keywords

Highlights

We present software and an analysis method to probe 3D grid codes using human fMRI

Based on an alignment score between 3D movement direction and grid orientation

We then tested this using a 3D virtual environment and fMRI

Signals in entorhinal cortex were explained by a face-centred cubic lattice model

Introduction

Grid cells in entorhinal cortex (EC) have received much attention from researchers in the field of spatial navigation because of their unique firing pattern. A grid cell fires at multiple periodic locations resembling a hexagon when an animal explores an environment (Hafting et al., 2005; Fig. 1A). Importantly, different grid cells have different spatial scales and phases, the combination of which enables efficient encoding of an entire space using relatively few cells, compared to when each individual cell fires at unique locations, as is the case with hippocampal place cells. More recently, electrophysiology studies found that grid cells do not only encode the physical location of animals but also encode a continuously changing auditory tone in rats (Aronov et al. 2017) and visual space in primates (Killian et al. 2012). Human fMRI studies have also observed grid-like signals that encode locations during mental imagery (Bellmund et al., 2016; Horner et al., 2016), features of abstract visual stimuli (Constantinescu et al., 2016) and eye position during 2D visual search (Nau et al., 2018; Julian et al., 2018). This suggests that grid cells may be suitable for more abstract "cognitive mapping" (Tolman, 1948). If grid cells are indeed involved in abstract cognitive mapping, the 'space' might not be limited to simple 2D physical space on which most grid cell research has to date been conducted, because cognitive tasks can involve more than two features or attributes. Grid cells should also be able to efficiently encode 3D and higher dimensional space (unless the high dimensional cognitive problem can be projected into low dimensional space, e.g. context-dependent encoding).

Mathematical studies predict that grid cells would fire at locations which correspond to the position of the centre of spheres tightly packed in 3D space, known as a face-centred cubic lattice (FCC), hexagonal close packing (HCP), or intermediate arrangements that yield the highest packing ratio (Mathis et al., 2015; Fig. 2). There are only a few mammals that naturally explore 3D volumetric space upon which experimenters can test such theoretical predictions, for example, bats or primates in an arboretum. Although at least one research group is currently testing grid cells in flying bats

(Ginosar et al., 2016), there is not yet clear empirical evidence of grid cells showing 3D lattice structures. Technical difficulties associated with recording animals freely moving in 3D space might be one reason for the dearth of empirical findings relating to 3D grid fields.

This is where studying the human brain becomes advantageous. With recent advances in affordable and easy-to-use virtual reality (VR) technologies, experimenters can create a virtual 3D world where human participants feel like they are floating or flying. A complex tethered or wireless recording device is not required for human participants in such a virtual environment. Although virtual environments have inherent limitations, such as lacking some primary sensory inputs, it is nevertheless a valuable starting point for studying the human brain in a volumetric 3D space and with which grid cells can be potentially probed. fMRI is the first choice to study grid cells in the human brain because it is non-invasive and can detect signals in a deep structure like EC. An obvious limitation of fMRI is that it does not have cellular resolution. Nevertheless, previous fMRI studies have successfully investigated grid cells in 2D space using a known property of grid cells whereby their activity is modulated by movement direction (Doeller et al., 2010). This property is central to the approach we describe here.

As discussed by Stangl et al. (2017), grid code analysis is non-trivial, even in 2D, with various analysis strategies employed by different researchers. Extending grid analysis into 3D requires additional theoretical and methodological considerations. Although this article does not aim to provide a complete review of grid analysis in the literature, we outline key methodological issues that are either unique to 3D or relevant to both 2D and 3D. Furthermore, we showcase graphical user interface (GUI) software that we developed to visualize 3D grid structure and direction-modulated grid signals.

In the Methods section we first explain the principles of detecting 3D grid codes (FCC and HCP models) using fMRI with the software we developed. A detailed description of the analysis method then follows. Next, we present our experimental paradigm that involved VR in zero gravity during fMRI where we test the grid cell models empirically in EC. Following this, in the Results section we report our findings from the fMRI study. We then discuss the methodological limitations and future directions for studying 3D grid signals.

Methods

Grid analysis

A principle for detecting 3D grid codes using fMRI

Before we propose a method for detecting 3D grid codes, we will first summarise how 2D grid codes have been probed in previous fMRI studies. fMRI measures the gross activity of thousands of neurons via complex neural-hemodynamic coupling. When the thousands of grid cells that fire at different locations are summed up, the gross activity is no longer expected to respond to fixed periodic locations in the environment. However, there is another important property of grid cells that enables their detection at a macroscopic level like fMRI (Doeller et al., 2010). The activity of 'conjunctive' grid cells is modulated by the alignment between the movement direction of an animal and the grid axis (Doeller et al., 2010). This means that a grid cell shows greater activity when an animal moves in directions parallel to one of the grid axes compared to other directions (Fig. 1B). As the majority of grid cells share a common grid axis, the summed response of thousands of grid cells can be systematically modulated by the movement direction of a participant. In previous studies that investigated grid cells in 2D, fMRI activity was modelled as a cosine function of movement direction relative to the grid axis with a period of 60 degrees to account for hexagonal symmetry (e.g. Doeller et al., 2010; Constantinescu et al., 2016). Another explanation for the direction-modulated grid signal measured by fMRI is that when a participant's movement direction is aligned with the main grid axis, relatively few grid cells are repeatedly activated, whereas when the movement is not

aligned with the main grid axis, more cells are irregularly activated. The fMRI response can be different in these two cases due to non-linear neural-hemodynamic coupling (e.g. Doeller et al., 2010).

We assume that the same principle of direction-modulation will hold in 3D, so that fMRI activity can be modelled as the degree of alignment between 3D movement direction and the grid axis. The question we face is how to define and predict the grid axis if grid cells have 3D receptive fields following either the FCC or HCP arrangements (Mathis et al., 2015; Stella and Treves, 2015). Both FCC and HCP arrangements are analogous to the spatial arrangement of tightly stacked spheres inside a box with a minimum gap (e.g. like oranges in a crate). These 3D arrangements can be viewed as 2D hexagonal lattices stacked on top of each other with a translational shift between the layers. FCC is composed of three repeating layers (blue, yellow and red spheres, see Fig. 2A,B) and HCP is composed of two repeating layers (blue and red spheres, see Fig. 2F,G). In both models, one centre sphere is surrounded by 12 neighbouring spheres (Fig. 2C,D,H,I). To enable ourselves and other researchers to visualize the 3D receptive fields of grid cells, we developed interactive web-based software where users can zoom, pan, rotate, and cross-sect the 3D arrangements (the software, including a manual, can be accessed here: www.fil.ion.ucl.ac.uk/Maguire/grid3D_gui). Example screenshots are shown in Fig. 3. The software was implemented using Unity 5.4 (Unity Technologies, CA, United States).

FCC is a pure lattice where the location of each node can be described by a linear combination of three basis vectors. The FCC arrangement is symmetric across the origin (e.g. the blue and yellow spheres are facing each other, Fig. 2C) and every grid field is surrounded by 12 grid fields in the same arrangement. Thus, it is intuitive to define the grid axis as the direction linking one grid field to its neighbouring grid fields (the green lines linking a centre black sphere to neighbouring coloured spheres in Fig. 2C,D). We can then model fMRI signal as a cosine of the angle between the 3D

movement direction and the nearest grid axis. Thus, a larger signal is expected when the angle is smaller (i.e. the movement is aligned to the grid axis). The nearest grid axis forms the minimum angle with the direction vector. We can predict the grid cell's response when a participant is moving in a particular 3D direction, defined by azimuth (horizontal angle) and pitch (vertical angle) using our interactive software (example screenshots are shown in Fig. 4A,B). Figure 2E shows the predicted grid activity as a function of azimuth and pitch of a movement direction relative to the grid axis.

Importantly, predicting the direction-modulated grid signal is not straightforward for the HCP model because HCP is not a pure lattice, as has been discussed in previous theoretical studies (Mathis et al., 2015; Stella and Treves, 2015). Unlike the FCC, the HCP arrangement is symmetric across the horizontal plane (e.g. the blue spheres on a layer above the red spheres are located at the identical positions as the blue spheres on the layer below, Fig. 2H). Therefore, the arrangement of unit grid fields is dependent on the layer (Fig. 2H and Fig. 2I are 60° rotated from each other). This means that the grid axis is defined only locally in HCP (Supplementary Fig. 1; note that this is more evident when viewing the 3D arrangements using our 3D visualization software). This imposes a limitation in predicting a direction-modulated fMRI signal which is dependent on the global grid axis. There is currently no empirical data on how fMRI signal will vary when receptive fields of grid cells follow a non-lattice structure. One can, nevertheless, attempt to model the grid voxel's activity for the HCP model using one set of locally defined grid axes (Fig. 2H) with the caveat in mind. This yields largely similar response patterns to the FCC model except for the difference in vertical symmetry (Fig. 2E and J).

The orientation of the grid axis relative to the environment

Crucially, the activity of a grid cell, or a grid voxel in fMRI, depends upon both the movement direction of a participant (which is known to experimenters) and the orientation of the grid axis relative to the 3D environment (which is unknown to experimenters). Fig. 5 describes two

hypothetical cases where a participant moves in the same direction but the grid axis is oriented differently. In Fig. 5A, a participant's movement direction (black arrow) is relatively closely aligned to the grid axis with an angular deviation of $14°$, resulting in high activity (the yellow bar graph). In Fig. 5B, due to a different orientation of the grid axis, the same movement direction is farther away from the grid axis with an angle of $35°$, resulting in low activity. The orientation of the grid axis can be numerically estimated by iteratively fitting the experimental data - a process we describe in a later section.

Unlike in 2D where the orientation of the grid axis can be specified by one polar angle from a reference direction (e.g. $20°$ from the north-south axis), the grid axis in 3D can in theory be rotated along any three arbitrary axes and the order of applying each rotation also matters (known as the non-commutative property of 3D rotation). Although users can explore these 3D rotation options in our software, we restricted the rotation of the 3D grid axis to only one axis so that six hexagonal grid fields (the red spheres in Fig. 5) remain parallel to the ground of the environment when we analyse our fMRI data. This restriction in the rotation axis can be justified by the fact that grid cells on a 2D horizontal surface show corresponding grid fields. This restriction is also required when comparing putative grid orientations across multiple voxels or multiple participants using a standard circular statistic like a von Mises distribution. Conducting the modelling process in this way simplifies it and reduces the computational cost and the risk of overfitting GLMs for hundreds of possible 3D rotations.

The relationship between the grid alignment score and fMRI activity

A grid voxel's activity is expected to be modulated by the degree of alignment between the movement direction and the grid axis, and we defined the grid alignment score as the cosine of the angle between the movement direction and the nearest grid axis. This is equivalent to the previous grid analysis in 2D which used parametric regressors of cosine and sine functions (Doeller et al., 2010;

Horner et al., 2016), except for a minor difference in that our method predicts more abrupt changes in grid alignment scores when the movement direction passes the midpoint of two neighbouring grid axes (Supplementary Fig. 2B,C). Of note, the precise form of the direction-modulated firing rate of grid cells is not known in either 2D or 3D. There is also additional complexity in measuring a grid cell's signal via neural-hemodynamic coupling. Therefore, it is also possible to model the grid voxel's activity with a non-sinusoidal function, like a linear, binary or even more complex functions (Supplementary Fig. 2D,E). The exact relationship between direction-modulated grid activity and the fMRI response should be examined in future studies, but for now we believe that our choice of modelling the fMRI signal with the cosine of the angle is a reasonable starting point, as it is in line with previous studies in 2D.

Estimating 3D grid orientation in fMRI data

In this section, we describe how to estimate 3D grid orientation from an fMRI time series. As explained earlier, the grid alignment score can be calculated as the cosine of the angle between the participant's movement direction (known to experimenters) and the nearest grid axis. The nearest grid axis is determined by the orientation of the grid axis relative to the environment, which is unknown to the experimenters (Fig. 5). In 2D, the grid activity can be modelled as a simple cosine function of the horizontal movement direction (φ) and the orientation of grid axis (ω), and the orientation (ω) can be estimated analytically by fitting cosine and sine functions in a GLM (e.g. a quadrature filter, Doeller et al., 2010):

$$\cos(60° \cdot \varphi - \omega) = \cos(60° \cdot \varphi) \cdot \cos(\omega) - \sin(60° \cdot \varphi) \cdot \sin(\omega)$$

However, a simple analytical function of azimuth (φ), pitch (θ) and the grid axis orientation (ω or more parameters) which can describe the grid alignment score in 3D is unknown. We, therefore, suggest a simple numerical method to estimate grid orientation as follows:

We first assume that the grid orientation is aligned at 0 degrees from a reference direction (e.g. parallel to the side wall of the environment) and then calculate the grid alignment score. This grid alignment vector is then convolved with the hemodynamic response function (SPM canonical hemodynamic response function). The resulting vector serves as a hypothetical grid voxel signal. We create a general linear model (GLM) which contains this predictive 3D grid signal and nuisance regressors that include six head motion realignment parameters and experiment-specific conditions like an occasional question and response period. The fMRI time series (after standard preprocessing) in each voxel and in each scanning session is then fitted with the GLM, and the outcomes - beta (regression coefficients) and adjusted R square values (Soch et al., 2018) - are saved for each voxel.

We then repeat the whole procedure with newly calculated grid alignment scores with different assumptions, namely that the grid orientation is aligned at 15, 30, 45, …, 120 degrees relative to the environment (note that we only need to sample the grid orientation up to 120 degrees, as the geometry of the 3D lattice structure of both FCC and HCP is symmetric for the 120 degree rotations on a plane). For each voxel and each scanning session, we select the orientation of the grid axis that gives the best fit by comparing the adjusted R square of these multiple GLMs. A GLM with the smallest adjusted R square and a positive regression coefficient for the grid signal regressor is selected. The reason we select the GLM with a positive regression coefficient is to avoid the inverted relationship between the hypothetical grid cell's signal and the fMRI response (e.g. when movement is more aligned to the grid axis, the fMRI signal is lower). In rare case (<10% of voxels in our empirical data – see later sections) where all grid orientation models yield a negative regression coefficient, we simply select the GLM with the smallest R square. To summarise, this iterative fitting process identifies which grid orientation best describes the fMRI signal in each voxel and in each scanning session.

Of note, we compared our numerical estimation method and the previous quadrature filter approach using simulated data in 2D (Supplementary Text 1). The simulation showed that both methods could detect grid-like signal equally well at reasonable signal-to-noise ratios and sampling resolutions.

Testing for a grid signal in the fMRI data

We then test whether each voxel shows a consistent 3D grid signal across different scanning sessions by quantifying the regression coefficient of the grid signal model. For instance, if the fMRI data in one scanning session (e.g. run 1) is best fitted with a grid model that aligns at 15 degrees, we measure the grid score as the beta of the same grid orientation (15 degrees) model in the another scanning session (e.g. run 3). The beta values of voxels in the brain region of interest (ROI) are averaged for each participant, and a t-test is used to test whether the beta is positive at the group level (excluding outliers, participants with more than a standard deviation of 3 in our empirical data). This approach is similar to previous 2D grid analyses where the grid orientation is estimated from one half of the dataset and is tested on the other half of the dataset, and the regression coefficient is analysed at the group level (e.g. Doeller et al., 2010; a standard group level inference for fMRI experiments).

However, there is a difference between our study and some of the previous studies in terms of grid orientation averaging. In Doeller at al. (2010) and Horner et al. (2016), the estimated grid orientation of each voxel within the EC ROI was averaged, and this averaged grid orientation model was tested in the other half of the data. Here, we estimate and test the grid orientation model within each voxel, then we later summarise the grid score of voxels within the ROI. Neighbouring grid cells share a common grid orientation which is the essential property of grid cells that allows the detection of the direction-modulated signal at the fMRI voxel level, and earlier fMRI studies assumed one unique grid orientation for the entire EC. However, there is also evidence of multiple grid modules in the EC that

have different grid orientations and scales (Stensola et al., 2012), and estimating and testing grid orientation at the voxel level, instead of the whole ROI, might maximise the sensitivity of analyses. This voxel-by-voxel estimation and test approach was used in a more recent 2D grid cell study (Nau et al., 2018).

Experimental protocol

In this section we describe an empirical fMRI experiment where data were acquired while participants were exploring a virtual 3D environment. The experimental paradigm included a pre-scanning session with VR goggles. We applied our proposed 3D grid analysis to this dataset. This empirical dataset has been reported in a separate paper which investigated vertical and horizontal head direction encoding outside of the EC (https://www.biorxiv.org/content/early/2018/05/31/335976), and is summarised here for the reader's convenience. The 3D grid code analysis reported in the current paper is novel and has not been published elsewhere.

Participants

Thirty healthy adults took part in the experiment (16 females; mean age 25.9±4.8 years; range 19-36 years; all right-handed). All had normal or corrected to normal vision and gave informed written consent to participation in accordance with the local research ethics committee.

The virtual environment

Participants were instructed that they were exploring a virtual zero-gravity environment, called "spaceship", where they could move freely up, down, forwards and backwards. This spaceship had two rectangular compartments linked by a corridor (Fig. 6A, the environment can also be viewed in our online software). Participants could orient themselves in each compartment because the visual appearance of the walls differed (e.g. a window on the west side and a grey wall on the east side;

the ceilings and floors also had different textures or hues). A snapshot of this virtual spaceship as seen from a participant's perspective is shown in Fig. 6B,C. The virtual environment was implemented using Unity 5.4 (Unity Technologies, CA, United States).

The virtual spaceship was rendered on two different mediums for pre-scanning tasks and scanning tasks respectively: a head-mounted VR display (Samsung Gear VR, model: SM-R322 with Samsung Galaxy S6 phone) and a standard computer screen (Dell Optiplex 980 with an integrated graphic chipset). The VR display was used because it has been suggested that prior vestibular experience with a VR environment can later reinstate the relevant body-based cues during fMRI scanning, when only visual input is available due to head immobilisation (Shine et al., 2016). The VR head-mounted display provided participants with a fully immersive sensation of 3D space via its head motion tracking system, stereoscopic vision and a wide field-of-view (96°). A rotation movement in the VR display was made by a participant's physical head rotation and a translational movement was made by a button press on the Bluetooth controller (SteelSeries Stratus XL, Denmark). For example, a participant could move up to the ceiling in the virtual spaceship by physically looking above and pressing the forward button. To rotate to the right, they physically rotated their head to the right or rotated their whole body when the required rotation was beyond the range of motion for neck rotation. For ease of rotation, participants were seated on a swivel chair.

During fMRI scanning, participants watched a video rendered on a standard computer screen (aspect ratio=4:3, Fig. 6C). The video was a first-person perspective that gave the participants the feeling of moving in a virtual spaceship. The stimuli were projected on the screen using a projector at the back of the MRI scanner bore (Epson EH-TW5900 projector), and participants saw the screen through a mirror attached to the head coil. The screen covered a field of view of ~19° horizontally and ~14° vertically.

Pre-scan: VR memory task

Wearing the VR display, participants freely explored the environment (5 minutes) and then performed a spatial memory test (15 minutes) where they had to recall the location of balls by physically directing their head to the remembered locations (Fig. 6B). During the memory task, on each trial participants encoded the location of a floating ball by looking at it from different directions and distances for 18 seconds. Immediately after the encoding phase, participants were transported to a random fixed location and then had to look at the remembered location of the ball. They received feedback (angular error in degrees) after they made their decision. There were 16 main trials where participants had to locate the ball within the same compartment. We also added extra 6 trials where participants were asked to point a ball's location across the wall from a different room. These trials were included to encourage participants to encode a global map of the environment.

fMRI scan: direction judgment task during passive viewing

During scanning, participants watched a video rendered on a standard display and performed a direction judgment task. The video provided participants with the feeling that they were flying in a controlled 3D trajectory within the spaceship (Fig. 6C). The pre-programmed video allowed tight control of location, direction and timing for all participants. The trajectory consisted of multiple short linear movements (each of 3 seconds) followed by rotation (2/2.6 seconds). We restricted the range of movement directions (-60 to 60 degree with 30 degree steps, both vertically and horizontally, indicated by arrows in Fig. 6C) to increase the frequency of each movement direction visited within the limited scanning duration. All participants followed the same trajectory without abrupt rotations where each of 25 directions (5 levels of pitch x 5 levels of azimuth) was evenly sampled (min = 18, max = 20 trials). A constant linear and angular velocity was applied in order to control velocity, which can also influence grid cells' activity. If a participant reached the boundary of the spaceship, a blank screen appeared for 2 seconds and then a trajectory started again from the other end of the spaceship. For 25% of the time, a question screen appeared immediately after a

linear movement and participants indicated the direction of their last movement by pressing an MR-compatible button pad (a 5-alternative forced choice question with a time limit of 5 seconds; Fig. 6C). Vertical or horizontal questions were randomly presented. This direction judgment task was used to ensure participants kept track of their movements during scanning. The two compartments of the spaceship were visited alternatively for each of 4 scanning sessions. Half of the participants started in one compartment and half started in the other compartment. Each scanning session lasted ~11 minutes with a short break between the sessions, making a total functional scanning time of ~50 min.

Post-scan debriefing

After scanning, participants were debriefed about how much they felt immersed in the virtual environment during the pre-scan session with VR head mounted display and during scanning. Participants chose from multiple options: "I felt like I was really in the spaceship"; "I occasionally thought about the environment as being computer-generated, but overall the environment was convincing and I felt I was moving around in the spaceship"; "I was often distracted by the feeling that I was not in a real environment".

Behavioural analyses

For the pre-scan memory task, we report the mean angular deviation for the main trials (where participants had to look towards the remembered location of the ball within the same compartment of the environment). We then report the overall accuracy of the direction judgment task during scanning (chance=20%) to check whether participants knew in which direction they were moving in the 3D environment. . Further data and analyses related to the vertical and horizontal direction sensitivity, are available in preprint form here (https://www.biorxiv.org/content/early/2018/05/31/335976). For the debriefing question, we counted the number of responses for each option.

Scanning and pre-processing

T2*-weighted echo planar images (EPI) were acquired using a 3T Siemens Trio scanner (Siemens, Erlangen, Germany) with a 32-channel head coil. Scanning parameters optimised for reducing susceptibility-induced signal loss in areas near the orbitofrontal cortex and medial temporal lobe were used: 44 transverse slices angled at -30°, TR=3.08 s, TE=30 ms, resolution=3×3x3mm, matrix size=64x74, z-shim gradient moment of -0.4mT/m ms (Weiskopf et al. 2006). Fieldmaps were acquired with a standard manufacturer's double echo gradient echo field map sequence (short TE=10 ms, long TE=12.46 ms, 64 axial slices with 2 mm thickness and 1 mm gap yielding whole brain coverage; in-plane resolution 3 x 3 mm). After the functional scans, a 3D MDEFT structural scan was obtained with 1mm isotropic resolution.

Preprocessing of data was performed using SPM12 (www.fil.ion.ucl.ac.uk/spm). The first 5 volumes from each functional session were discarded to allow for T1 equilibration effects. The remaining functional images were realigned to the first volume of each run and geometric distortion was corrected by the SPM unwarp function using the fieldmaps. Each participant's anatomical image was then coregistered to the distortion corrected mean functional images. Functional images were normalised to MNI space and smoothed with 6mm kernel.

ROI selection

We used anatomical ROIs, left and right EC masks (Fig. 7A). The ROIs were manually delineated on the group-averaged MRI scans from a previous independent study on 3D space representation (Kim et al., 2017) following the protocol in Pruessner et al. (2002). The number of functional voxels (3 x 3 x 3 mm) within the ROI masks was 47 (left) and 49 (right). Of note, EC was further divided into posterior medial and anterior lateral parts in one previous fMRI study (Bellmund et al., 2016), based on the finding in rodents that grid cells are typically reported in the medial EC. However, our study used standard resolution fMRI and further segmentation of this kind was not feasible. Functional

specialisation within the EC is an interesting topic that needs to be further addressed in future studies with high-resolution scanning sequences.

Another important consideration for selecting EC ROIs is that EC is notoriously difficult to image because of fMRI susceptibility artefact in this vicinity. Although sequence development continues in this regard, EC still has inherently low raw BOLD signal compared to other cortical regions. Crucially, standard fMRI analysis software like SPM excludes voxels of low signal by default. The "global masking threshold" parameter in the first-level model specification in SPM determines which voxels are to be included in the analysis based on the raw intensity, and EC voxels can often be excluded. It can also result in a different number of voxels in an EC ROI for each participant. We caution researchers about excluding voxels for two reasons. First, an exclusion criterion based on the mean BOLD intensity can be arbitrary. Depending on the version of the software, some voxels can be included or excluded from the analysis. Second, raw BOLD intensity alone does not predict whether a voxel shows functional modulation. For instance, whereas the raw signal intensity of cerebrospinal fluid (CSF) is higher than most other cortical areas, we rarely observe meaningful signals in the CSF in typical cognitive experimental paradigms. In our study, we defined the EC ROIs purely anatomically, without excluding any voxels based on raw signal intensity.

Main grid analysis

We applied the 3D grid analysis that we described in detail above to the preprocessed fMRI dataset. In essence, we estimated the orientation of the 3D grid axis for the FCC model in each voxel and scanning session by iteratively fitting the fMRI time series to the predicted grid alignment score defined as the cosine of movement direction and the nearest grid axis. The grid model was tested on another scanning session. Because our virtual spaceship had two compartments, we trained and tested the grid cell models within each compartment, and averaged the regression coefficient of the two compartments.

We then tested whether the estimated grid orientation of the FCC model was clustered across voxels within participants or across multiple participants. To test the voxel-wise clustering within participants, we calculated the percentage distribution of angular distance between the circular mean grid orientation and the estimated grid orientation of each voxel within ROIs in each participant (=histogram with bins centred at -45, -30, -15, 0, 15, 30, 45, 60 degree difference in putative grid orientation). If the grid orientation was clustered across voxels, this distribution would be non-uniformly distributed with the mode centred at 0. We averaged the angular distance distribution across participants, then applied a V-test for non-uniformity. To test the clustering across participants, we applied a Rayleigh test for non-uniformity to the circular mean grid orientation across participants. If the grid axis was anchored to visual features in the environment such as landmarks or the boundary, every participant would exhibit a similar grid orientation. The circular mean and non-uniformity test was computed using CircStat2012a toolbox (Berens, 2009). We normalised the grid orientation into 2*pi radians before we applied the V-test or Rayleigh test because the putative grid orientation was defined between 0 to 120 degrees whereas standard circular statistics is applied for 0 to 360 degrees.

We also tested whether the HCP grid model explained signal in the EC despite the methodological limitation which we explained earlier.

Control analysis – direction or view encoding model

Our 3D grid analysis (as well as the 2D grid analyses in the literature) relies on the dependency of the neural signal on movement direction, and one concern is whether a neural signal that is responsive to one particular direction (or the view associated with a direction) could be weakly correlated with a grid model and so identified as a grid signal. This was why we used a direction (or view) encoding model as a control analysis. We created a direction-sensitive model signal which was sensitive to one

of nine 3D directions that were visited by participants in a virtual environment. The nine directions were regularly sampled both horizontally and vertically: (azimuth, pitch in degrees) = (-60, -60), (-60, 0), (-60, 60), (0, -60), (0, 0), (0, 60), (60, -60), (60, 0), (60, 60). Following Bellmund et al. (2016), we assumed that each direction-sensitive neural response had a margin of 30 degrees. This meant that neurons or voxels that responded strongly to (0, 0) direction would also respond strongly to (±30, ±30), and would respond weakly to the rest of the movement directions. We convolved the binary direction response vector with the hemodynamic response function. We created a GLM similar to the grid cell model described in the previous section but now the grid signal was replaced by the direction encoding signal. Again, the best direction-encoding model was selected for each voxel from one scanning session and then tested on a different scanning session. If voxels in our ROIs (left and right EC) responded to unique directions, we would see a significantly positive regression coefficient for a direction model at the group level.

Control analyses – other grid models

In 2D, a non-hexagonal grid model, such as a 4-fold symmetry, has been used as a control model (Doeller et al. 2010). Similarly, we tested whether fMRI signal in the EC was explained by a square lattice model (Fig. 8A). A square lattice model has a lower packing density than the FCC and HCP models, so the square lattice model is not an optimal way of encoding 3D space. Just as in our testing of the FCC and HCP models, we assumed that the activity of a grid voxel was modulated by the alignment score (cosine of angle) between movement direction and the grid axis orientation (Fig. 8A).

We also tested a hexagonal grid model which was only responsive to the horizontal axis ("Azimuth-only"). This model is related to the previous observation in rats that receptive fields of grid cells were vertically elongated in a spiral staircase apparatus (Hayman et al. 2011) (Fig. 8B). We know nothing about whether or not there are direction-modulated signals when grid cells have such

anisotropic receptive fields, but we think it is reasonable to assume that grid activity would be only modulated by the horizontal angle between movement direction and the grid axis, independent of pitch, in this case (Fig. 8B). For example, grid activity would be high if a participant moves in a 0°, 60°, 120°, 180°, 240°, 300° direction (azimuth-wise) independent of whether they move up or down.

Control analysis – a primary auditory cortex ROI

We tested the FCC grid model in a size-matched control brain region (primary auditory cortex) to reassure that the grid-like representation we identified in EC was not merely an artefact that was present across the whole brain. We defined a spherical ROI (radius 7mm, 51 voxels) centred at a peak coordinate [-44, -24, 8] from the fMRI meta-analysis toolbox Neurosynth using the key words "primary auditory" (Yarkoni et al. 2011) (Fig. 7A).

Empirical results

Behavioural

During the pre-scan memory task, participants were reasonably successful at locating a ball's position (mean error 21°, SD 9°, Fig. 6B). The mean accuracy of direction judgments during scanning was well above chance level (mean 74%, SD 16%; chance 20%), suggesting that participants knew their 3D movement direction in the virtual environment during scanning.

The rating data showed that participants felt immersed in the virtual environment, with the vast majority choosing either "I felt like I was really in the spaceship" (57% for the pre-scan VR head mounted display task, 10% for the scanning task) or "I occasionally thought about the environment as being on a computer screen, but overall the environment was convincing and I felt I was moving around in the spaceship" (43% for the pre-scan VR head mounted didplay task, 80% for the scanning task). This result implies that our virtual environment effectively conveyed a sense of being in 3D space.

fMRI – main grid analysis

We tested whether fMRI signal in the left and right EC was modulated by participants' 3D direction as predicted by the FCC lattice model. The FCC grid model was significant in the left EC (t(28)=2.6, p=0.008, one-sided), and showed a trend in the right EC (t(28)=1.7, p=0.054, one-sided) (Fig. 7B).

The putative FCC grid orientation of each voxel was clustered around the mean orientation within participants (V-test in the left EC, V=33.6, p=$1.0*10^{-7}$; the right EC, V=30.5, p=$7.9*10^{-6}$, Fig. 7C) similar to previous studies (Nau et al., 2018; Julian et al., 2018). Of note, the current study, as well as the previous studies, used spatially smoothed fMRI data (which is common practice in fMRI analysis to increase SNR). Therefore, spatial smoothing could have contributed to the clustering of grid orientation across neighbouring voxels in EC.

By contrast, the mean grid orientation was not significantly clustered across participants (Rayleigh's test for non-uniformity in the left EC, room A, z=1.6, p=0.2; room B, z=1.5, p=0.2; the right EC, room A, z=1.6, p=0.2; room B, z= 0.3, p=0.8, Fig. 7C), suggesting that the grid axis was not anchored to, or driven by, particular features of the environment. This non-clustered grid orientation across participants is consistent with previous studies which used a circular arena (Doeller et al., 2010; Nau et al., 2018). Of note, Julian et al. (2018) observed a clustering of grid orientation around 7.5 degrees to the cardinal axis (modulo 15 degree) for a square arena, but not for a rectangular environment that was similar to that of our spaceship.

We also tested the HCP grid model with the assumption that the fMRI signal is modulated by the local grid axis. The HCP model did not significantly explain the response of either EC (the left EC, t(29)=0.4, p=0.3, the right EC, t(29)=0.4, p=0.3, one-sided, Fig. 7D). However, as we explained in the Methods, an fMRI analysis that rely on a direction-modulated grid signal is not ideal for detecting

the HCP model because it lacks a global grid axis. Thus, a further comparison between the FCC and HCP models requires future electrophysiological studies that can directly assess the receptive fields of grid cells.

fMRI – control analyses

To exclude the possibility of a neural signal sensitive to one particular direction (or associated view) being identified as a grid voxel, we tested a unique direction encoding model as a control. The direction encoding model was not significant in either EC (left EC, t(29)=-1.8, p=0.9; right EC, t(29)=-1.5, p=0.9, one-sided, Fig. 7E), suggesting that the FCC grid-like signal that we observed in the EC was not driven by one particular direction.

We also tested a square lattice model and an azimuth-only model where vertical pitch was ignored. Neither of these models significantly explained the fMRI signal in the EC (square lattice model: left EC, t(29)=-1.1, p=0.9; right EC, t(29)=-0.7, p=0.7; azimuth-only model: left EC, t(29)=1.0, p=0.2; right EC, t(29)=1.0, p=0.2, one-sided, Fig. 7E).

Finally, the FCC grid model was not significant in the size-matched control ROI (primary auditory cortex, t(29)=0.6, p=0.6, one-sided), suggesting that the FCC grid-like signal that we identified in the EC was not a spurious effect that was detectable anywhere in the brain (Fig. 7B).

Discussion

Here we presented a VR experimental paradigm and a novel analysis method to investigate 3D grid codes non-invasively in humans. We also developed associated software to help researchers visualize 3D receptive fields of grid cells and predict their responses. Using these methods, in our empirical data we observed an fMRI signal in the EC which was in line with one particular 3D grid

model – an FCC lattice model. Here we discuss the implications and limitations of our study and make suggestions for future studies on 3D grid codes.

A prerequisite for probing a 3D grid code is to use an appropriate 3D environment. 3D lattice structures, like FCC or HCP, are optimal for encoding volumetric space (Mathis et al., 2015), and the existence of substructures like 2D walls or a 1D track could affect the response of grid cells. For instance, grid cells recorded in rats moving on a sloped terrain showed firing pattern similar to a 2D horizontal plane rather than a 3D lattice pattern (Hayman et al., 2015). Therefore, we built a fully volumetric virtual "zero-gravity" environment where participants could move freely in all directions. Furthermore, we complemented the fMRI scanning, where only visual input was available because of in-scanner head immobilisation, by using a VR head mounted display during pre-scan tasks as in Shine et al. (2016). We believe this pre-scan experience of physical head rotation when using the VR head mounted display was particularly helpful to participants in building the mental and neural representation of a 3D space, and this was supported by participants' reports in the debriefing session at the end of the experiment.

The main finding of this study relates to our probing of putative grid cells using fMRI by predicting the neural signal as a function of 3D movement direction and the grid axis. The principle of measuring direction-modulated grid signals has been widely used in 2D (Doeller et al., 2010; Constantinescu et al., 2016; Bellmund et al., 2016). However, in our study, we extended, for the first time, this principle into 3D volumetric space, thereby opening up the possibility of empirically studying grid cells in high-dimensional space. Predicting the activity of a grid cell was inevitably more complicated in 3D due to the added dimension, as we described in earlier. Consequently, we estimated the 3D grid orientation by iteratively fitting the neural data with signals predicted by different possible grid orientations. We successfully demonstrated the feasibility of this analysis

approach by finding our data was concordant with the FCC model in the left EC, the candidate brain structure for 3D grid encoding.

Our result is suggestive of grid cells responses exhibiting FCC lattice encoding in the human EC when participants explore a volumetric space, but we remain cautious until this finding is corroborated by future studies that directly measure cellular responses. It is not yet proven that the direction modulation principle also holds in 3D because there is no clear evidence of grid cells showing a regular 3D lattice pattern (of note, a recent study in bats found multiple firing fields that were not perfectly regular; Ginosar et al., 2016). Invasive recordings from the human brain in a similar 3D virtual reality experiment to the one we used here may be able to provide more direct evidence of grid cells with 3D receptive fields. Once there is a fuller understanding of the cellular physiology of grid cells, it will be possible to determine the optimal fMRI analysis protocol by considering the multiple factors we have described here, such as whether the orientation of the 3D grid axis is parallel to the ground or not, the precise model between the grid alignment and the fMRI signal (e.g. cosine, linear, binary), and the distribution of the grid orientation across different voxels within EC.

The FCC and HCP models should also be compared in future empirical studies. A theoretical study showed that both have identical encoding efficiency (Mathis et al., 2015). Stella and Treves (2015) found that simulated grid fields did not perfectly converge on either FCC or HCP alone, and the outcome had a small deviation from both models. Despite the equal likelihood of the two grid models at the cellular level, we found that detecting the HCP grid signal using direction-modulated fMRI signal is not as straightforward as detecting the FCC model because of the absence of global grid axes in the HCP model. Indeed, we did not find significant a HCP grid-like signal in our empirical data. We do not claim the superiority of the FCC model over HCP model given the methodological issue of direction-modulation with the HCP model. The two models would be best compared using electrophysiological methods, as they can circumvent the issue of grid axis and the direction-

modulation. If future studies reveal unequivocal dominance of one model over the other, it would be interesting to investigate how factors such as the anisotropy of the environment (all animals are influenced by gravity, thus the vertical axis is distinguished from the other two axes) might influence the optimal encoding of space. Furthermore, grid cells are known to be influenced by the geometry of environments (Krupic et al., 2014). Here, we used a spaceship with a rectangular shape, and so 3D grid models should be tested in environments of different shapes (e.g. spherical or asymmetric shapes) in the future.

Future studies examining 3D grid codes should also use active movement paradigms that sample all possible movement directions. In the current study, participants were passively moved during scanning for ease of controlling movement trajectories and to achieve even sampling of each 3D direction. Although previous fMRI studies have successfully observed grid signals using imagination tasks without active self-motion (Bellmund et al., 2016; Horner et al., 2016), it is known that passive movement disrupts velocity-modulated theta and grid firing in rodents (Winter et al., 2015). Self-motion signals are therefore critical for path integration associated with grid cells (McNaughton et al. 2006) and, consequently, more robust grid signals might be detected if active (virtual) movement paradigms are employed. One might also improve the power of detecting grid signals by sampling all 3D directions. In the present experiment, we only sampled movement directions spanning 120° vertically and horizontally due to limited scanning time. This limited sampling caused unbalanced data when investigating individual directional responses relative to the grid axis (e.g. participant A moved 0° to 120° relative to the putative grid orientation whereas participant B moved -30° to 90° relative to the grid orientation).

In summary, we believe that our experimental paradigm, analysis method and software serve as a useful initial stepping-stone for studying grid cells in realistic 3D worlds. Animal electrophysiology and human fMRI studies also suggest that a grid code is employed to encode not only physical space,

but also more abstract knowledge (Aronov et al., 2017; Constantinescu et al., 2016; Nau et al., 2018; Julian et al., 2018), and we hope our approach will in due course also encourage interrogation of abstract high-dimensional cognitive processes.

Acknowledgements

The authors declare no competing financial interests.

References

Aronov, D., Nevers, R., Tank, D.W., 2017. Mapping of a non-spatial dimension by the hippocampal–entorhinal circuit. Nature. 543, 719–722.

Bellmund, J.L., Deuker, L., Navarro Schröder, T., Doeller, CF., 2016. Grid-cell representations in mental simulation. eLife. 5, e17089.

Berens, P., 2009. CircStat : A *MATLAB* Toolbox for Circular Statistics. J. Stat. Softw. 31.

Constantinescu, A.O., O'Reilly, J.X., Behrens, T.E.J., 2016. Organizing conceptual knowledge in humans with a gridlike code. Science. 352, 1464–1468.

Doeller, C.F., Barry, C., Burgess, N., 2010. Evidence for grid cells in a human memory network. Nature. 463, 657–661.

Hafting, T., Fyhn, M., Molden, S., Moser, M.-B., Moser, E.I., 2005. Microstructure of a spatial map in the entorhinal cortex. Nature. 436, 801–806.

Horner, A.J., Bisby, J.A., Zotow, E., Bush, D., Burgess, N., 2016. Grid-like processing of imagined navigation. Curr. Biol. 26, 842–847.

Ginosar, G., Finkelstein, A., Las, L., Ulanovsky, N., 2016. Representation of 3D space in the entorhinal cortex of flying bats, Society for Neuroscience abstract, San Diego, USA.

Julian, J.B., Keinath, A.T., Frazzetta, G., Epstein, R.A., 2018. Human entorhinal cortex represents visual space using a boundary-anchored grid. Nat. Neurosci. 21, 191-194.

Killian, N.J., Jutras, M.J., Buffalo, E.A., 2012. A map of visual space in the primate entorhinal cortex. Nature. 491, 761–764.

Krupic, J., Bauza, M., Burton, S., Lever, C., O'Keefe, J., 2014. How environment geometry affects grid cell symmetry and what we can learn from it. Philos. Trans. R. Soc. B Biol. Sci. 369, 20130188.

Mathis, A., Stemmier, M.B., Herz, A.V.M., 2015. Probable nature of higher-dimensional symmetries underlying mammalian grid-cell activity patterns. eLife. 4, e05979

McNaughton, B.L., Battaglia, F.P., Jensen, O., Moser, E.I., Moser, M.-B., 2006. Path integration and the neural basis of the "cognitive map." Nat. Rev. Neurosci. 7, 663–678.

Nau, M., Navarro Schröder, T., Bellmund, J.L.S., Doeller, C.F., 2018. Hexadirectional coding of visual space in human entorhinal cortex. Nat. Neurosci. 21, 188-190.

Pruessner, J.C., Köhler, S., Crane, J., Pruessner, M., Lord, C., Byrne, A., Kabani, N., Collins, D.L., Evans, A.C., 2002. Volumetry of temporopolar, perirhinal, entorhinal and parahippocampal cortex from high-resolution MR images: considering the variability of the collateral sulcus. Cereb. Cortex. 12, 1342–1353.

Stangl, M., Shine, J., Wolbers, T., 2017. The GridCAT: A toolbox for automated analysis of human grid cell codes in fMRI. Front. Neuroinform. 11, 1–12.

Shine, J.P., Valdes-Herrera, J.P., Hegarty, M., Wolbers T., 2016. The human retrosplenial cortex and thalamus code head direction in a global reference frame. J. Neurosci. 36, 6371–6381.

Soch, J., Allefeld, C., 2018. MACS – a new SPM toolbox for model assessment, comparison and selection. J. Neurosci. Methods. 306, 19–31.

Stella, F., Treves, A., 2015. The self-organization of grid cells in 3D. eLife, 4, e05913.

Stensola, H., Stensola, T., Solstad, T., FrØland, K., Moser, M.-B., Moser, E.I., 2012. The entorhinal grid map is discretized. Nature. 492, 72–78.

Tolman, E.C., 1948. Cognitive maps in rats and men. Psychol. Rev. 55, 189–208.

Weiskopf, N., Hutton, C., Josephs, O., Deichmann, R., 2006. Optimal EPI parameters for reduction of susceptibility-induced BOLD sensitivity losses: a whole-brain analysis at 3 T and 1.5 T. Neuroimage. 33, 493–504.

Winter, S.S., Mehlman, M.L., Clark, B.J., Taube, J.S., 2015. Passive transport disrupts grid signals in the parahippocampal cortex. Curr. Biol. 25, 2493–2502.

Yarkoni, T., Poldrack, R.A., Nichols, T.E., Van Essen, D.C., Wager, T.D., 2011. Large-scale automated synthesis of human functional neuroimaging data. Nat. Methods. 8, 665–670.

A.

B.
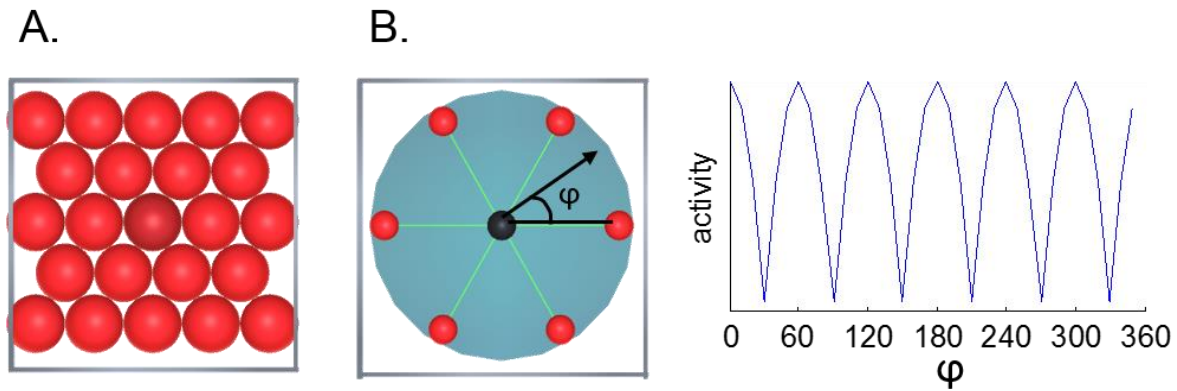
Fig 1. 2D grid cells. **A.** A grid cell fires at multiple locations (called grid fields, red circles) which correspond to the centre of circles closely fitted in a 2D box. **B.** A grid cell's activity is modulated by the animal's movement direction (black arrow) relative to the grid axis (green lines linking one grid field to its neighbouring six grid fields). φ denotes the angle between the movement direction and the grid axis. The grid cell fires more when an animal's moving direction is aligned to one of the grid axes. A grid axis is regularly displaced with 60° periodicity (right panel), therefore, a grid cell's activity also shows a periodic response pattern depending on the animal's movement direction.
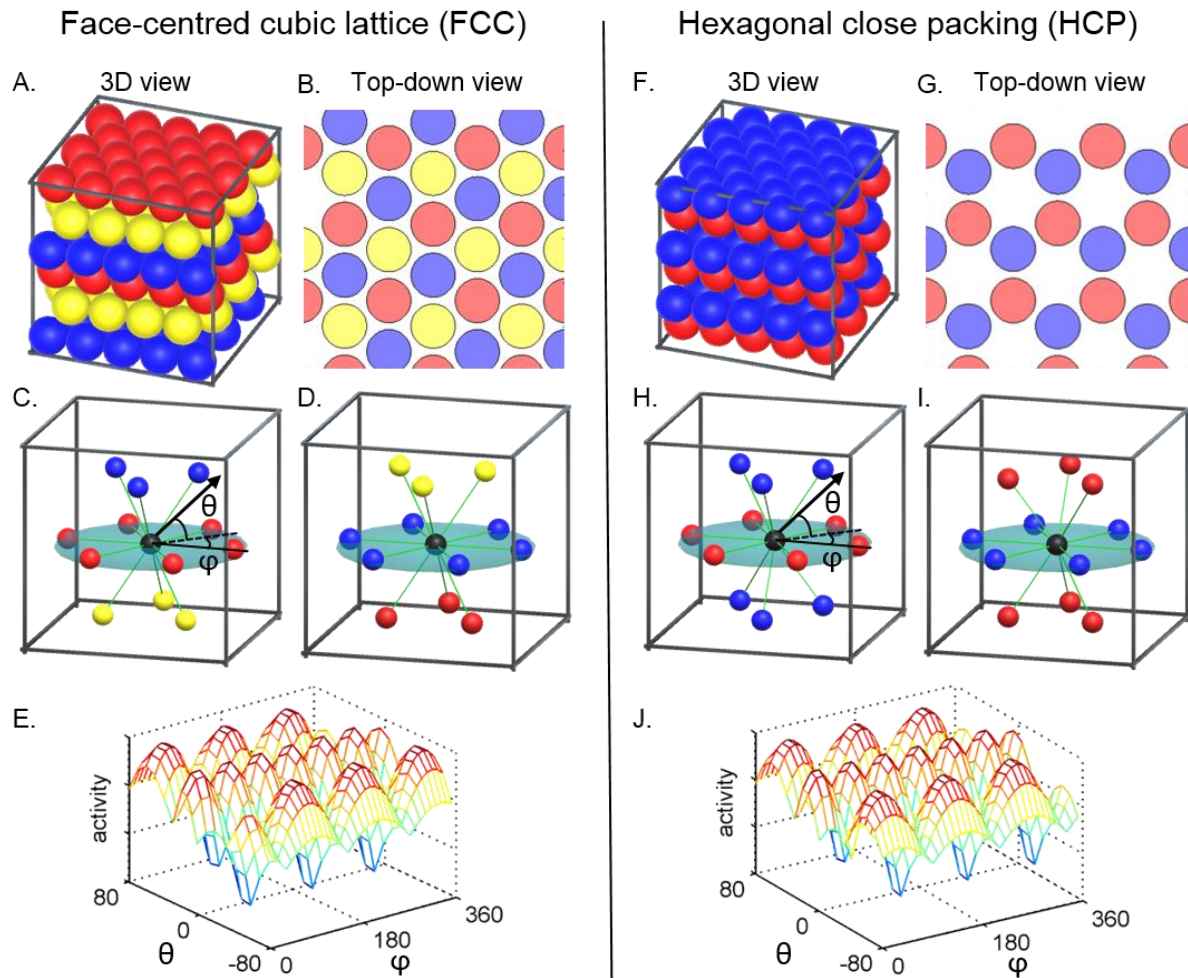
Fig. 2. FCC and HCP models. A grid cell is proposed to fire at multiple 3D locations (called grid fields, coloured spheres) which correspond to the centre of spheres closely fitted in a box (**A,F**). The FCC and HCP arrangements have equally high packing density. The 3D arrangements can be viewed as 2D hexagonal lattices stacked on top of each other with a translational shift between the layers. FCC is composed of three repeating layers (blue, yellow and red spheres) and HCP is composed of two repeating layers (blue and red). The top-down views show spheres of reduced radius for visualization purposes (**B,G**). Grid axes are shown as green lines linking one grid field to the neighbouring 12 grid fields (**C,D,H,I**). FCC is a pure lattice in the mathematical sense, that is symmetric along the origin (e.g. blue and yellow spheres are symmetric (**C**), and can be described by three basis vectors. Thus, every sphere is surrounded by other spheres in the same arrangement, e.g. a sphere on the red layer (**C**) and a sphere on the blue layer (**D**). HCP lacks such symmetry (e.g. blue spheres on the top layer and bottom layer are not symmetric across the origin (**H**). The 3D arrangement of a unit cell is different for different layers, e.g. a sphere on the red layer (**H**) and a sphere on the blue layer (**I**) are surrounded by spheres that are 60° rotated from each other. Therefore, a grid axis can be defined only locally in HCP. Similar to a grid cell in 2D, it is expected that a grid cell's activity is modulated by the alignment between an animal's movement direction (black arrow) and the grid axis (green lines) (**C,D,H,I**). Depending on the vertical (θ) and horizontal (φ) component of the movement direction relative to the grid axis, a grid cell's activity is expected to show a complex pattern of responses (**E,J**).
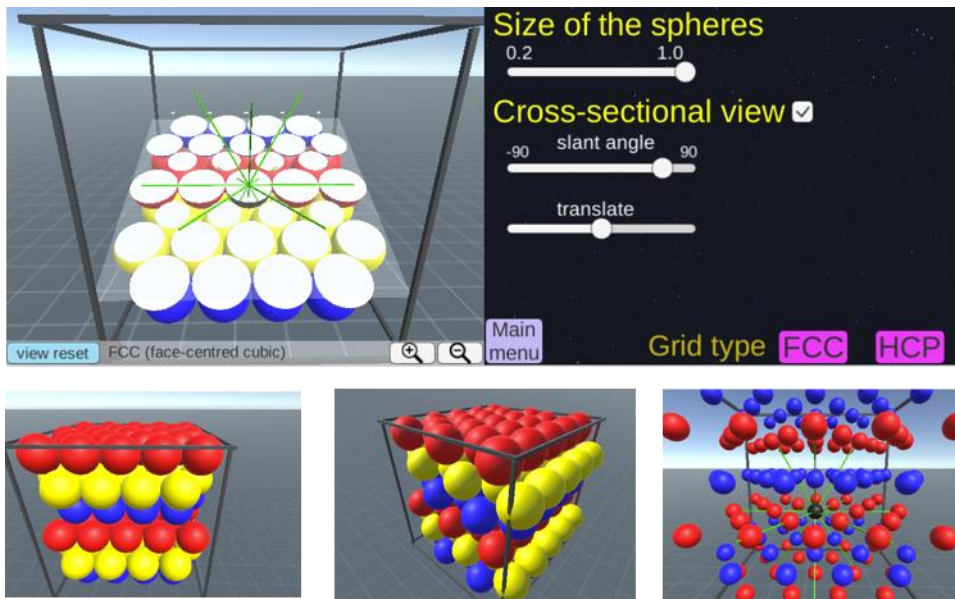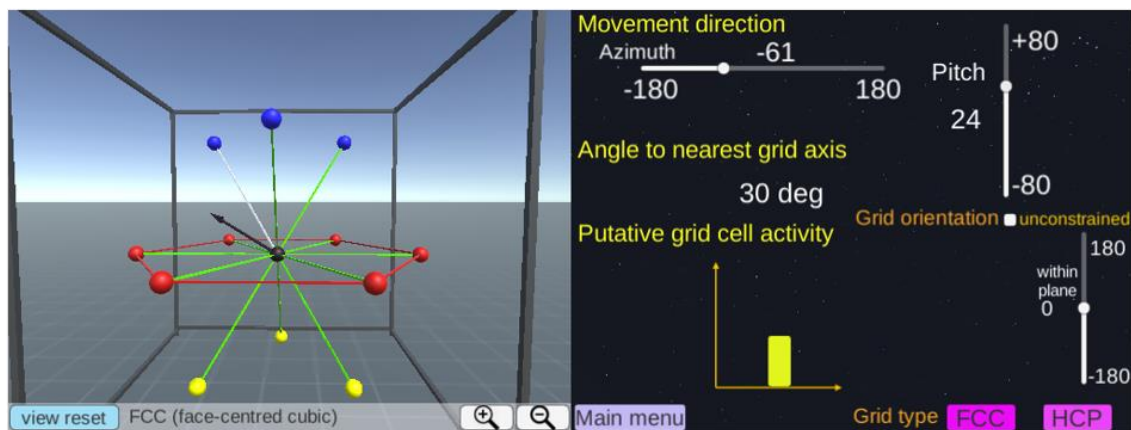
Fig. 3. Screenshots of our 3D grid fields visualization software. The software, including a manual, can be accessed here: www.fil.ion.ucl.ac.uk/Maguire/grid3D_gui. Users can change the viewpoint, the size of the spheres, and select cross-sectional views of grid fields. Users can also switch between the FCC and HCP arrangements.
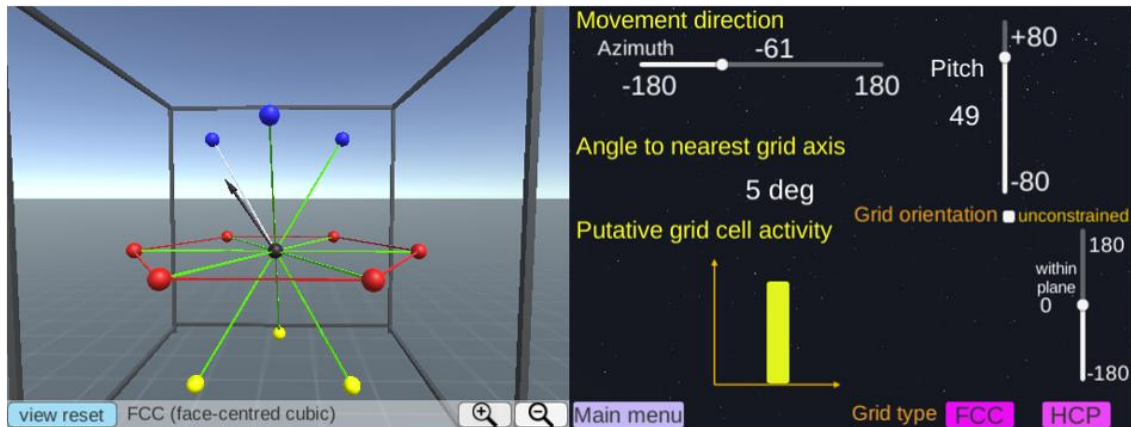
Fig. 4. A grid cell's activity is modulated by the movement direction relative to the grid axis. **A.** A participant's 3D movement direction (black arrow, left panel) is close to the grid axis (white line, left panel) with 5° deviation. Thus, the activity of grid cells is expected to be high (yellow bar graph, right panel). **B.** A participant's movement direction (black arrow, left panel) is far away from the grid axis (white line, left panel) with 30° deviation. Consequently, less activity is expected (yellow bar graph, right panel). Users can change the movement direction using the sliders on the right panel. Users can also switch between the FCC and HCP models and change the viewpoint.

A. Grid axis orientation=17°
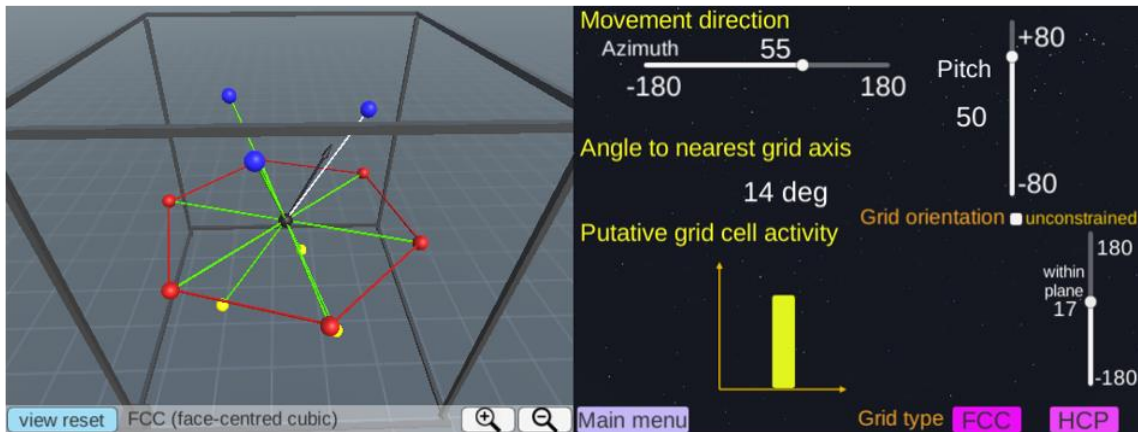
B. Grid axis orientation=56°
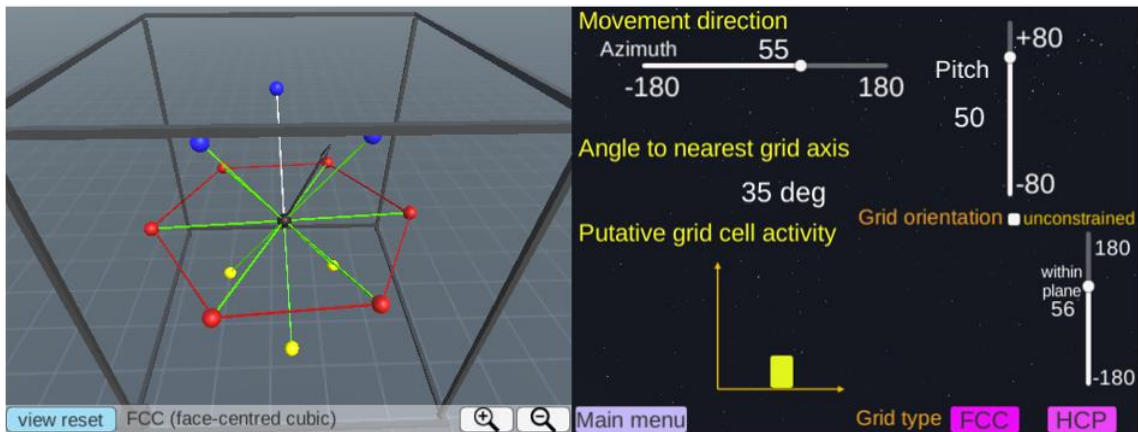
Fig. 5. The orientation of the grid axis relative to the environment. The movement direction (black arrow, left panel) is identical in **A** and **B** (azimuth=55°, pitch=50° in this example). However, grid cells are aligned differently relative to the environment (rectangular frame, left panels in **A** and **B**), meaning that the grid axes are rotated from each other (left panel). Thus, the grid alignment scores measured as the angle between the movement direction and the nearest grid axis differ (14° versus 35°), resulting in different amounts of grid activity (yellow bars graph, right panels in **A** and **B**). Users can change the orientation of the grid axis using the sliders on the right panel.
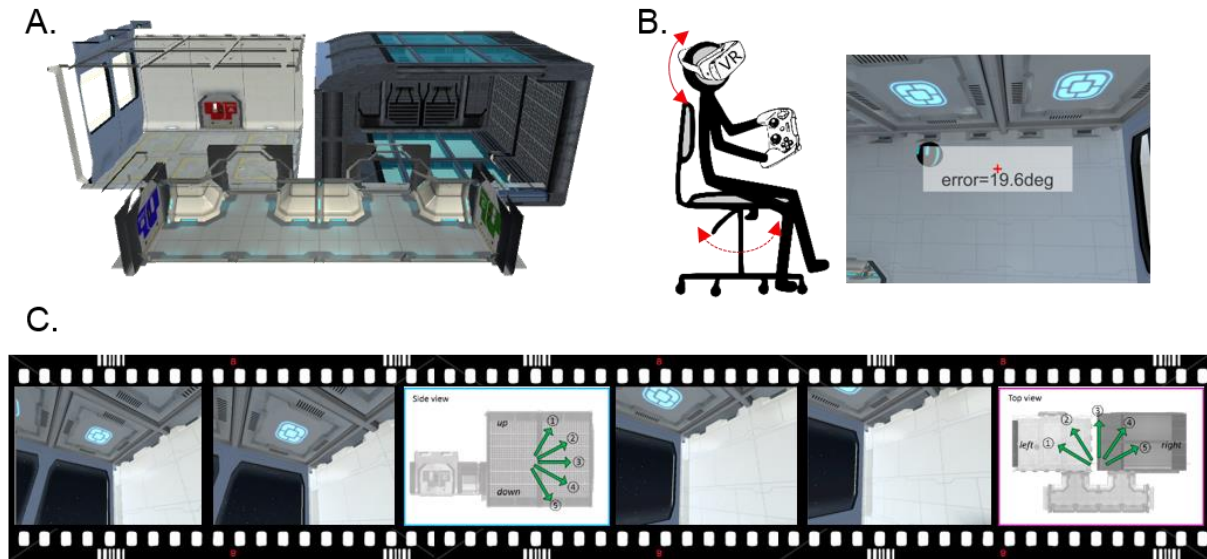
Fig. 6. The empirical experiment. **A.** A side view showing the layout of the virtual 3D spaceship. **B.** Prior to scanning, participants explored the 3D environment while wearing a virtual reality head mounted display. **C.** During scanning, participants viewed a video rendered on a standard display. The video provided the feeling that participants were flying in a 3D trajectory within the spaceship. Participants occasionally indicated, via a keypad response, their vertical and horizontal movement direction when questioned.
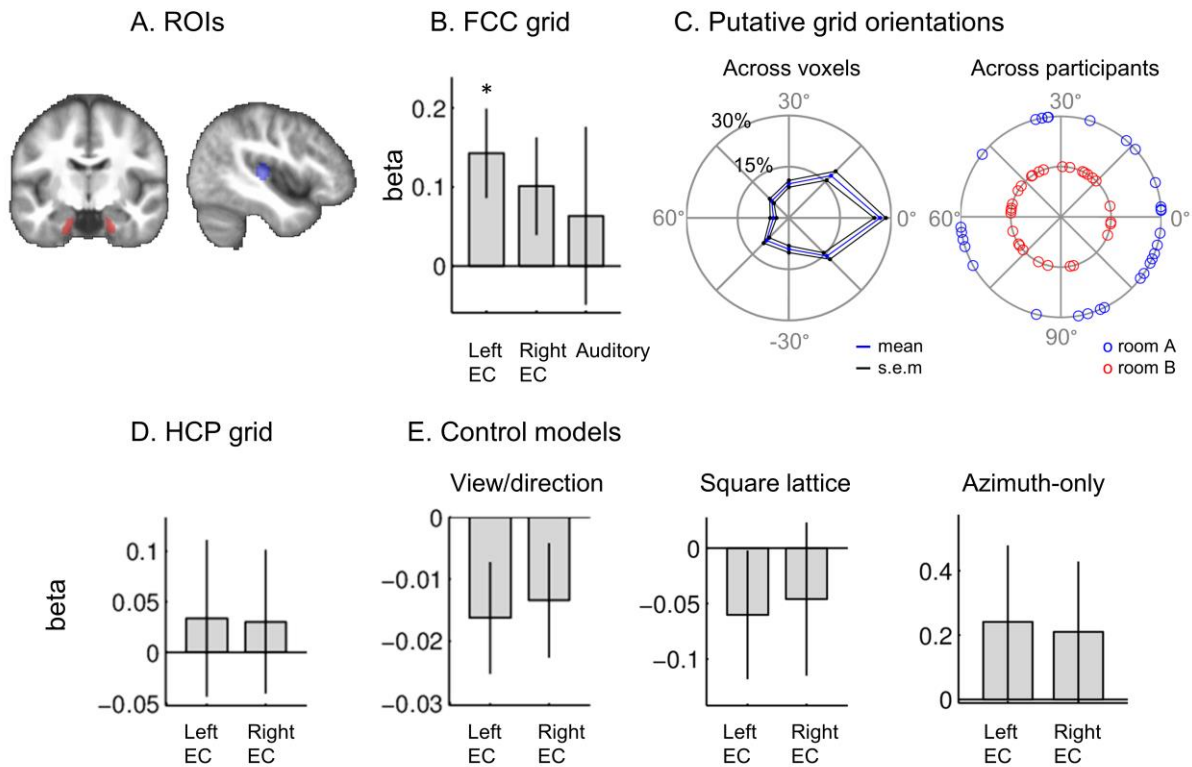
Fig. 7. 3D grid-like representations in the left EC. **A.** Bilateral EC (red) and a primary auditory cortex (blue) ROIs are shown on the group-averaged structural MRI scan. **B.** The mean beta of the FCC grid cell model was significantly positive in the left EC. There was a similar trend in the right EC (p=0.054), but not in the control brain region – the auditory cortex. **C.** Putative FCC grid orientation in the left EC was clustered around the mean grid orientation within participants (the left rose plot), but random across participants (the right polar plot). **D.** The HCP model was not significant in either EC (see the main text for a methodological limitation related to this). **E.** Control models (view or direction encoding models, a square lattice model and an azimuth-only grid model) were also not significant in the EC. *p<0.01. The error bars are SEM.
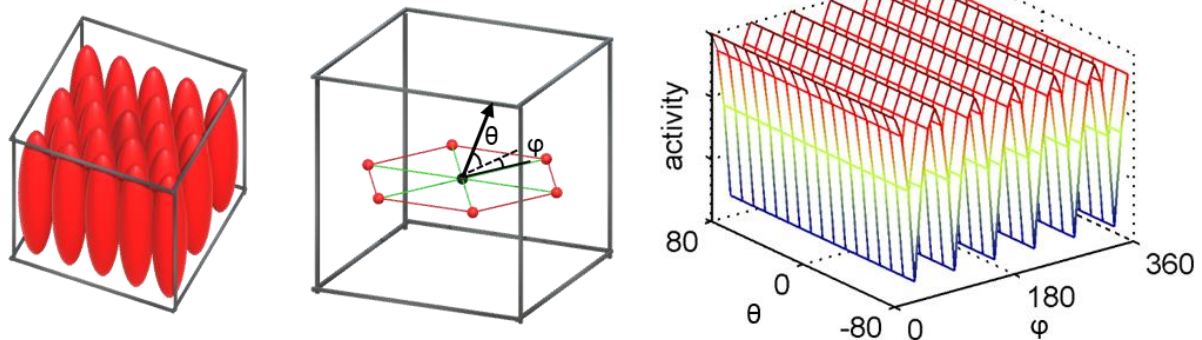
Fig. 8. Control grid models. **A.** Receptive fields of hypothetical grid cells which follow a square lattice arrangement (the left panel). The grid activity is expected to be modulated by the movement direction (the black arrow) relative to the orthogonal grid axis (the green lines, the middle panel). It displays 90 degree periodicity for azimuth (φ) when vertical pitch (θ) is close to zero (the right panel). **B.** Receptive fields of hypothetical grid cells which show hexagonal periodicity only along the horizontal axes and not along the vertical axis (the left panel). The grid activity is expected to be modulated by the horizontal movement (φ) independent of whether a participant is moving up or down (θ, the middle and the right panels).
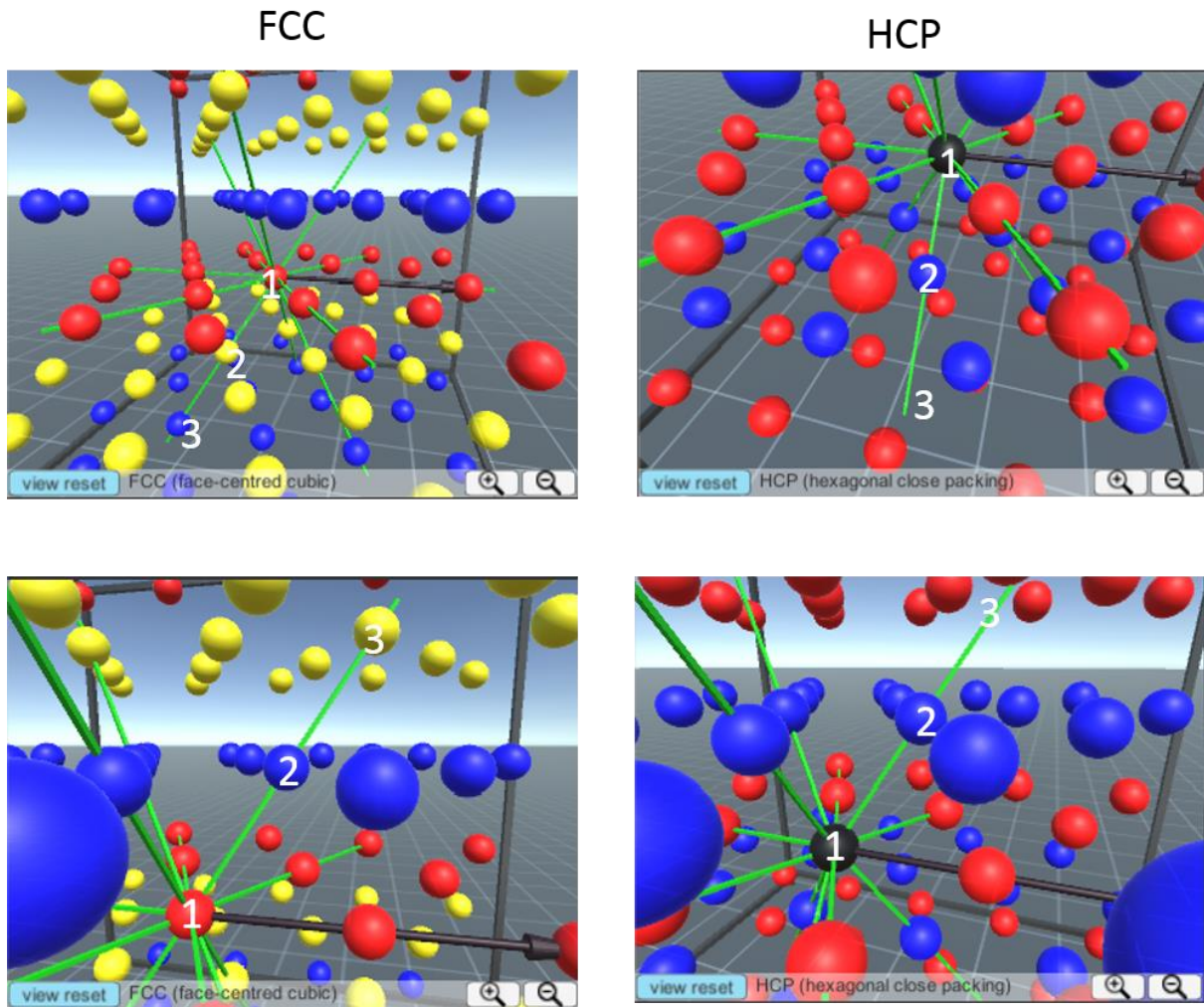
Supplementary Material

3D grid codes in human entorhinal cortex: Theoretical and methodological considerations and fMRI findings

Misun Kim, Eleanor A. Maguire

Wellcome Centre for Human Neuroimaging, Institute of Neurology, University College London, London WC1N 3AR, UK

Supplementary Fig. 1. Grid axes of the FCC and HCP arrangements.

FCC is a pure lattice with centre-symmetry. If one moves along the main grid axis from one node, every grid field will be passed (three nodes labelled as '1', '2', '3' in this example). In contrast, HCP does not have such symmetry. When one moves in the locally-defined grid axis, the grid field at the next layer is not passed ('3' does not pass the centre of the grid fields). It is easier to appreciate this 3D arrangement by using our visualization software (www.fil.ion.ucl.ac.uk/~mkim/grid3D_ver01).
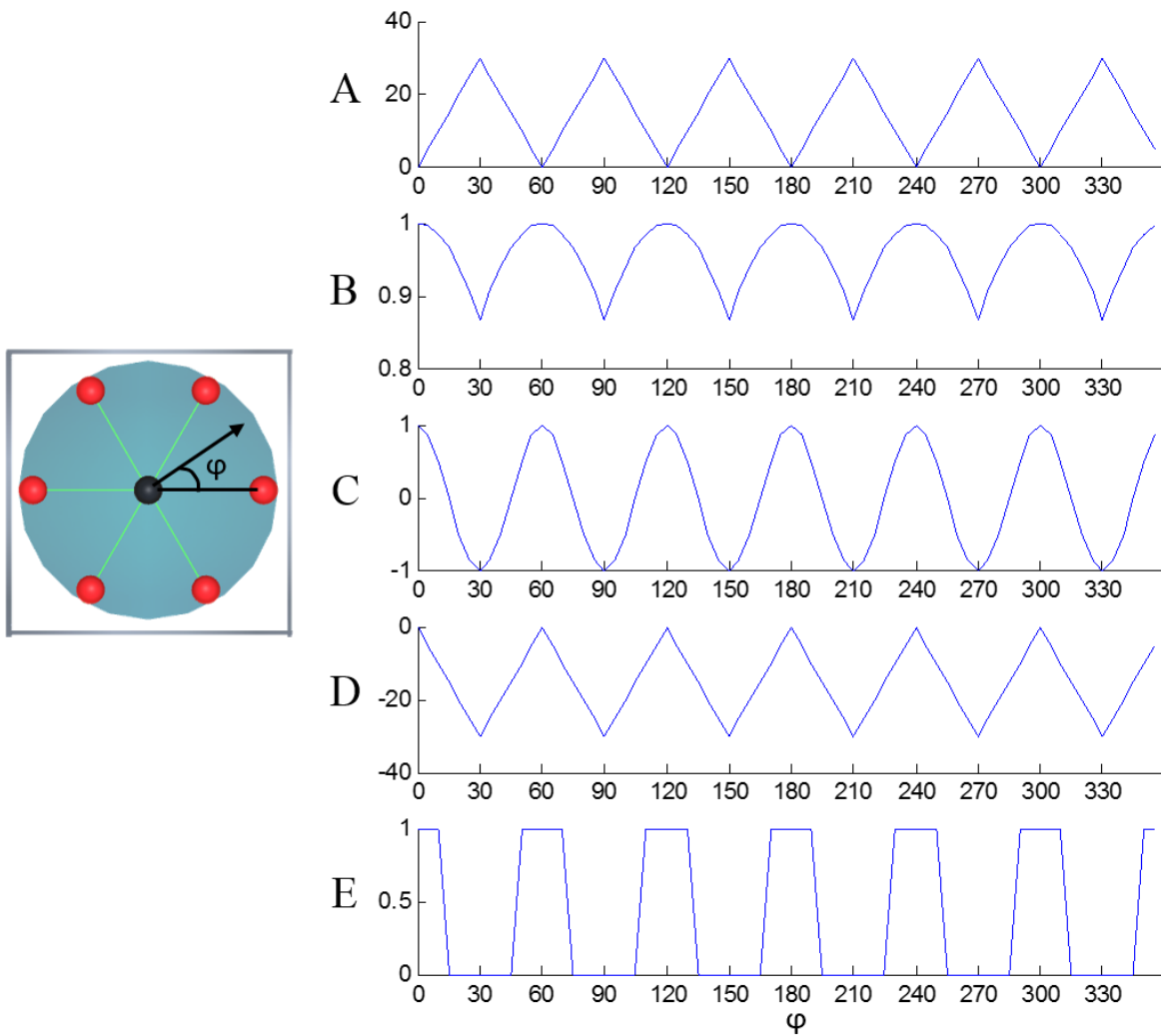
Supplementary Fig. 2. Possible relationships between grid alignment and the fMRI signal.

A. An angle between the movement direction (black arrow) and the nearest grid axis (green lines). **B.** A cosine of the nearest angle. **C.** A sinusoidal signal with a periodicity of 60 degrees. **D.** A linear signal (the negative of the nearest angle). **E.** A binary signal.

Supplementary Text 1. Comparison of numerical estimation and quadrature filter approaches in simulated 2D grid signals.

Introduction

In this simulation, we generated synthetic 2D grid signals to test whether our numerical grid orientation estimation method can detect such signals. We compared how well the numerical estimation methods with different sampling resolutions and a previous analytic approach (the quadrature filter, e.g. Doeller et al. 2010) detected the grid signal in the presence of noise.

Methods

We first created two virtual direction trajectories (approximating two scanning sessions of 10 minutes length each) where the range of movement (θ) was restricted to $[-60°, 60°]$, similar to our empirical data (see Supplementary Fig. 3 below). Next, we computed the grid alignment score vector by assigning random grid orientations (φ) for 30 virtual participants using the formula, $\cos(6*(\theta - \varphi))$. This hypothetical grid cell activity was convolved with a canonical hemodynamic response function and then Gaussian noise of varying size (SNR=1, 0.1, 0.01) was added.

In the numerical estimation method, we iteratively fitted the hypothetical grid signals when different grid orientations were assumed (either 15°, 7.5° or 1° resolution) and selected the grid orientation which had the best fit to the actual data in each scanning session (see details in the main text). We tested whether the grid model selected in the first session resulted in a positive regression coefficient in the second session and vice versa (a one-sided t-test). For the quadrature filter approach, we estimated the grid orientation (φ) using the regression coefficient of $\cos(6*\theta)$ and $\sin(6*\theta)$ regressors, $\varphi=\arctan(b1/b2)$ for each scanning session. We tested whether a new cosine regressor with the grid orientation estimated from the first session resulted in a positive regression coefficient in the second session and vice versa.

Results

Supplementary Fig. 4 below shows group mean grid scores (beta) and R-square values for varying SNR. All numerical estimation methods and quadrature filter approaches could reliably detect the grid signal when SNR was high (Supplementary Fig. 4A, 15°, $t(29)=33.5$, $p<0.001$; 7.5°, $t(29)=55.0$, $p<0.001$; 1°, $t(29)=97.3$, $p<0.001$, quadrature, $t(29)=98.1$, $p<0.001$) or middle (Supplementary Fig. 4B, 15°, $t(29)=5.3$, $p<0.001$; 7.5°, $t(29)=4.9$, $p<0.001$; 1°, $t(29)=5.0$, $p<0.001$, quadrature, $t(29)=5.1$,

p<0.001). None of the methods could detect the grid signal if the SNR was low (Supplementary Fig. 4C, 15°, t(29)=0.0, p=0.5; 7.5°, t(29)=-0.2, p=0.6; 1°, t(29)=-0.2, p=0.6, quadrature, t(29)=-0.2, p=0.6).

When SNR was high, the quadrature filter approach and numerical method with fine sampling resolution (1°, which virtually converges to an analytic solution) was better at detecting a grid signal compared to the numerical method with coarser sampling resolution (7.5°, 15°), in terms of a higher grid score and R-square (Supplementary Fig. 4A, grid score, F(3,87)=18.8, p<0.001; R-square, F(3,87)=27.9, p<0.001). This was due to discretized estimates of the grid orientation when coarser sampling resolution was used.

The numerical methods with varying sampling resolution and the quadrature filter approach showed similar grid scores and R-square values when SNR was middle (Supplementary Fig. 4B, grid score, F(3,87)=1.3, p=0.3; R-square, F(3,87)=1.0, p=0.4) or low (Supplementary Fig. 4C, grid score, F(3,87)=0.7, p=0.6; R-square, F(3,87)=2.2, p=0.1).

Discussion

Both analytic methods and numerical methods could detect underlying grid signals if the noise level was not too high. The analytic method and a numerical method with fine sampling resolution performed better than a numerical method with coarse sampling resolution if SNR was high. Real fMRI data is often noisy (e.g. the adjusted R-square value of our actual data in the entorhinal cortex was only 0.15) and the sampling resolution of the numerical method might have a negligible effect on detecting grid signal. Indeed, FCC grid scores in our actual fMRI data were comparable when we estimated the grid orientation with either 15° or 7.5° resolution.
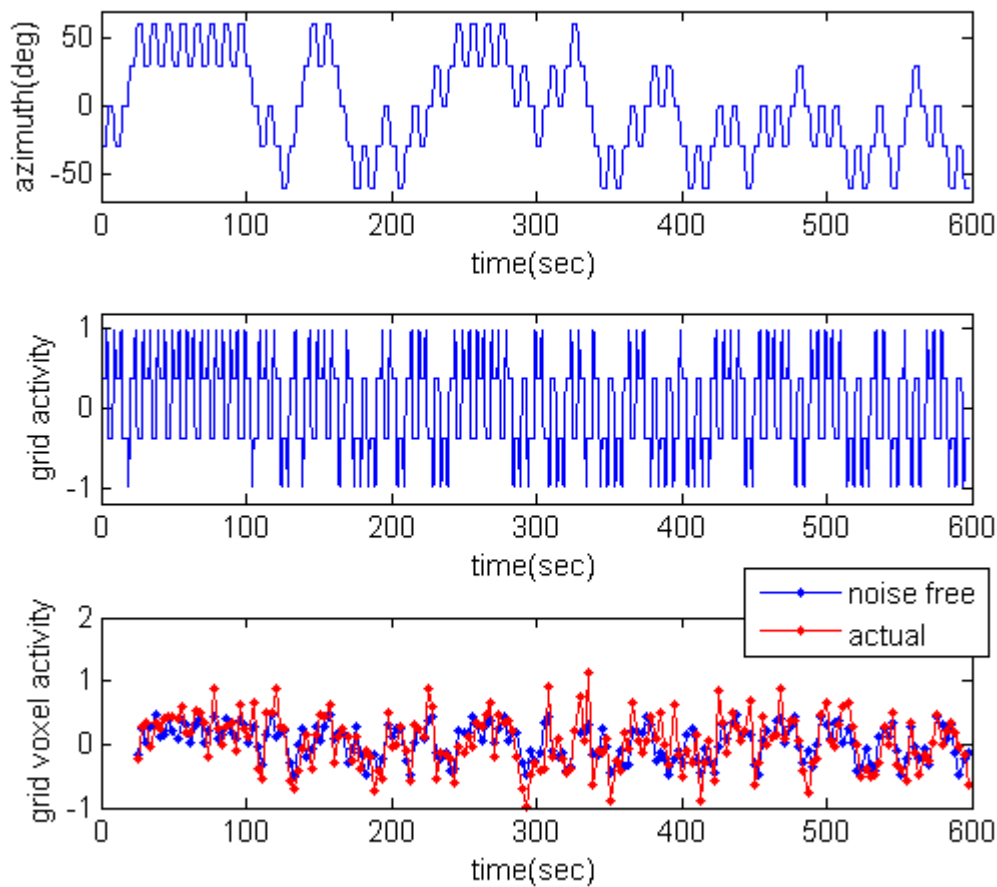
Supplementary Fig. 3. Simulated grid cell activity. Top panel, virtual movement trajectory of a participant. Middle panel, hypothetical grid cell activity of one participant whose grid orientation (φ) was 41°. Bottom panel, hypothetical grid cell activity was convolved with a hemodynamic response function, resulting in grid voxel activity. Before ("noise free") and after ("actual") the addition of Gaussian noise (SNR=1).
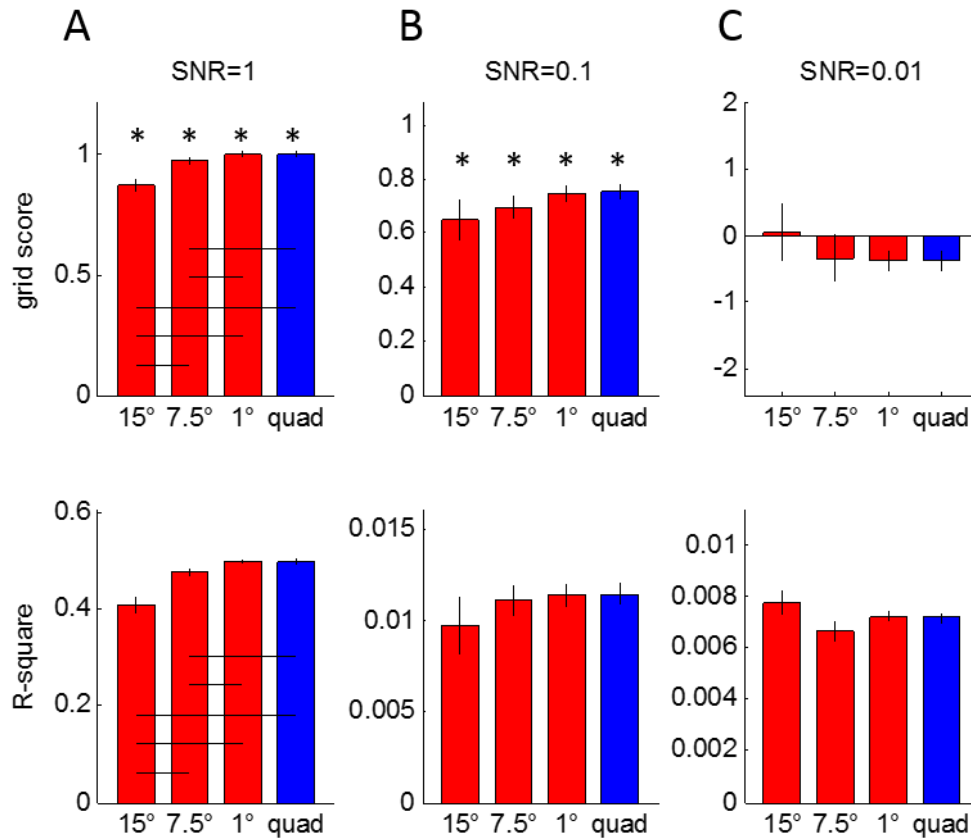
Supplementary Fig. 4. Comparison of the numerical estimation and quadrature filter approaches in 2D simulated data. When SNR was relatively high (**A** and **B**), both numerical and filter approaches correctly revealed the grid signal (positive grid score). When SNR was low (**C**), neither of the methods recovered the grid signal. Quadrature filter approaches or the numerical estimation with fine resolution (1°) were more sensitive to detecting grid-like signals than numerical estimation methods with coarse sampling resolutions (15°, 7.5°), only when SNR was high (**A**). All methods yielded similar results when SNR was middle or low (**B** and **C**). *$p<0.05$. Black horizontal bars indicate a significant difference between the conditions (post-hoc pairwise t-tests). Error bars are standard error adjusted for a within-subjects design.